# A Hierarchical Electromagnetic-Circuit Technique for Statistical Analysis of RF Circuits in the Spectral Domain

Arun V. Sathanur, *Student Member, IEEE*, Ritochit Chakraborty, and Vikram Jandhyala, *Senior Member, IEEE*

***Abstract*—Spectral domain statistical analysis of RF circuits, combining a circuit simulator, which models the circuit part and a full-wave field solver, which models the passive elements, is presented in this paper. This paper first illustrates the importance of the knowledge of correlation information in accurately modeling the probability density functions (PDFs) of eventual objective functions using a simple transmission line paradigm. Next, this paper looks at the statistical study of on-chip RF passives using the spiral inductor as an example. It is shown that larger process variations necessitate modeling by means of a quadratic response surface to preserve accuracy. This results in nonindependent non-Gaussian nonclosed-form PDFs for the equivalent-circuit parameters of the passives. This paper then proposes a hierarchical technique to perform statistical analysis of RF circuits based on $y$-parameter representation for the circuit and the passive element parts. The proposed technique obviates the need for optimization steps to derive the equivalent-circuit parameters for the electromagnetic objects and the need to compute the correlation matrix between the circuit equivalent elements, while maintaining accuracy. The proposed approach is illustrated for the statistical analysis of an RF amplifier and its differential version operating at 15.78 GHz. PDFs of various quantities of interest are derived and yield measures are computed.**

***Index Terms*—Correlation, electromagnetic field solver, Monte Carlo, probability distribution function, process variations, RF circuits, spiral inductors, yield, $y$-parameters.**

## I. Introduction

THE increasing need for higher data rates is continuously pushing the carrier frequencies of communication systems higher. This trend is complemented by the scaling down of device and interconnect dimensions that enables enhanced functionality on a single chip. The flip side of this is the increasing susceptibility of circuits to process variations which produce lower yields. It is imperative that accurate modeling schemes be developed in order to capture the impact of process variations on the performance of circuits [1]. For RF circuits, process variations affect the on-chip performance of both active and passive components. This necessitates the inclusion of the effect of these variations on distributed interconnect based passives in modeling overall circuit performance. Full-wave electromagnetic (EM) analysis is required to accurately model the on-chip passives commensurate with the increasing frequencies of operation.

There has been a lot of work on statistical methods applied to circuit and interconnect performance measures. One category of work looks at the problems of clock skew and timing analysis in digital circuits [2]–[5]. The second category addresses the problem of estimating the yield of the circuits based on performance metrics like gain, slew rate, power, and noise figure under process variations, and are primarily aimed at analog and mixed signal circuits.

The work described in this paper falls into the second category. The approach in [6] uses a combination of analytical techniques and response surface methodology (RSM) to predict the statistical behavior of performance measures from the distributions of lower level process parameters. In another approach [7], response surfaces have been used with a technology computer-aided design (CAD) approach to determine the spread of circuit performance measures. In a recent work [8], the issues pertaining to asymptotic evaluation of the probability density function (PDF) of a random variable that can be expressed as a second-order response surface have been addressed. The techniques used in this work significantly speed up PDF evaluation as compared to performing Monte Carlo analysis.

Compared to the literature on statistical variability in circuits, little work has been undertaken in the area of statistical study on the performance of devices and components requiring EM modeling although this is of equal importance in present day design for manufacturability analysis. The impact of variability on board level signal integrity has been addressed in [9]. In another work [10], a commercial field simulator and linear regression has been used to perform statistical analysis of filters on substrates. It has been found that for large standard deviations of parameters contributing to variability of on-chip passives, quadratic response surfaces are more appropriate. These lead to a noticeable deviation from the Gaussian profile for the desired objective functions. This observation is true for both circuit and EM variability [8], [11].

Specifically, there is no previous work that attempts to investigate the variability with respect to RF circuits, requiring the use of a full-wave field solver for accurate modeling of the passive components such as spiral inductors and transformers.

This paper illustrates, using a transmission line example, the importance of the correct correlation information between the

Manuscript received June 23, 2008; revised October 30, 2008. First published March 16, 2009; current version published April 08, 2009. This work was supported by the National Science Foundation (NSF) under Grant ECS-0093102 and Grant EEC-0203518.

The authors are with the Applied Computational Engineering Laboratory, Department of Electrical Engineering, University of Washington, Seattle, WA 98195 USA (e-mail: arunsv@u.washington.edu; ritochit@u.washington.edu; vj@u.washington.edu).

Color versions of one or more of the figures in this paper are available online at http://ieeexplore.ieee.org.

Digital Object Identifier 10.1109/TMTT.2009.2015068

0018-9480/$25.00 © 2009 IEEE

Authorized licensed use limited to: University of Washington Libraries. Downloaded on July 13, 2009 at 15:12 from IEEE Xplore. Restrictions apply.

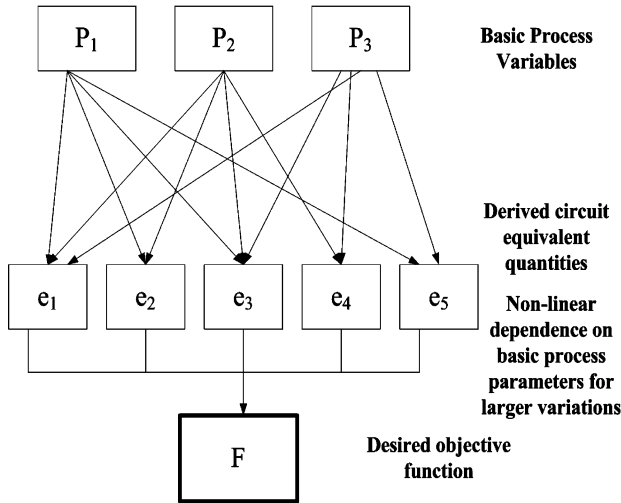


Fig. 1. Illustrating the general correlated and non-Gaussian nature of the derived circuit equivalent quantities.

derived circuit-equivalent quantities. It shows how the accurate statistical analysis of coupled circuit-EM systems can be performed without the need for extracting the correlation information and the optimization steps required to extract the derived circuit-equivalent quantities.

On-chip passive elements, though modeled by full-wave field solvers, are represented by equivalent circuits consisting of *R*, *L*, and *C* components to facilitate time-domain analysis. These element values are determined by means of numerical optimization or other extraction procedures from the $S$-parameters obtained through full-wave field solver simulations [12], [13]. Each of the equivalent-circuit elements will have a functional dependence on some or all of the basic process variables, which are relevant to the modeling of passive elements. Thus, the circuit element values are, in general, correlated. This is illustrated in Fig. 1.

Such *RLC* models are unsuitable for spectral domain statistical analysis of coupled circuit-EM systems because of the following issues.

- Variability in geometrical parameters such as metal width, metal thickness, oxide thickness, and electrical parameters such as substrate conductivity can be modeled accurately only by full-wave field solvers.
- The parameters that are important for field solver simulations are very different from those influencing the active circuit behavior and they cannot be used directly in the present framework for statistical analysis of circuits with SPICE-like simulators.
- Extra optimization steps are needed to synthesize the equivalent-circuit models.
- The need for accurate correlation matrices arises in order to guarantee the accuracy of the PDFs of higher level parameters such as gain and return loss.
- Only a certain class of multivariate PDFs can be uniquely specified by the mean vector and correlation matrix. The Gaussian PDF is one primary constituent of this class. For larger process variations, when the linear relationship is not true, it is not possible to define the joint PDF of the vector of derived circuit equivalent quantities in terms of the mean and correlation alone.

All these issues are addressed by the methodology outlined in this paper. This paper is organized as follows. Section II-A describes the transmission line paradigm to illustrate the effect of not modeling the correlation between derived variables. Section II-B looks at the statistical analysis of passive components with the spiral inductor as an example. Section III discusses the methodology developed in this paper. Section IV applies the methodology to compute the PDFs of quantities of interest in an RF amplifier and also extends the same to the differential version. Section V discusses the yield computation. Finally, Section VI concludes the paper and enumerates the further work to be undertaken in this direction.

## II. Non-Gaussian Nature of the PDFs and Associated Issues

### A. Transmission Line Paradigm

A transmission line example is used to illustrate how an erroneous PDF is produced by not modeling the correct correlation while using the derived variables. The transmission line considered in this example is a section of a microstrip with a nominal $Z_0$ (characteristic impedance) of 50 $\Omega$, terminated by a 50-$\Omega$ load. Empirical relations available in the literature [14] are used to compute the properties of interest. Hence, with this example, it becomes feasible to use Monte Carlo techniques for comparison purposes since full-wave field solver simulations are time intensive and not suitable for rapid Monte Carlo analysis. The quantity of interest is taken to be the absolute value of the input impedance ($|Z_{\text{in}}|$). The microstrip is subjected to process variations in the form of the width of the trace ($W$) and the permittivity ($\epsilon_r$) of the substrate between the trace and the ground plane. At their mean values, the nominal design of $Z_0 = 50\ \Omega$, and consequently, $|Z_{\text{in}}| = 50\ \Omega$ is produced.

Comparisons are now presented between various cases enumerated below, taking the PDF of $|Z_{\text{in}}|$ as the quantity of interest.

Case 1: Variations are in basic process parameters $W$ and $\epsilon_r$ with Gaussian PDF.

Case 2: Variations in $Z_0$ and $\beta$ assuming independence. These derived variables are not independent. This represents the case where the covariance matrix for the derived variables is not known, and therefore, as an approximation, assumed independent. The idea is to show that the resulting PDFs are erroneous if the derived variables are used without the knowledge of the covariance information.

Case 3: Variations in $Z_0$ and $\beta$, with the distribution taken to be the joint PDF defined by the mean and covariance matrix, which are obtained from a Monte Carlo analysis using the basic process parameters.

Fig. 2 represents the three cases enumerated above. The standard deviation is taken to be 0.03 of the mean for all the parameters. The curves corresponding to Cases 2 and 3 almost completely overlap.

Fig. 3 represents the same three cases, but this time for larger process variations. The standard deviation is taken to be 0.1 of

Authorized licensed use limited to: University of Washington Libraries. Downloaded on July 13, 2009 at 15:12 from IEEE Xplore. Restrictions apply.

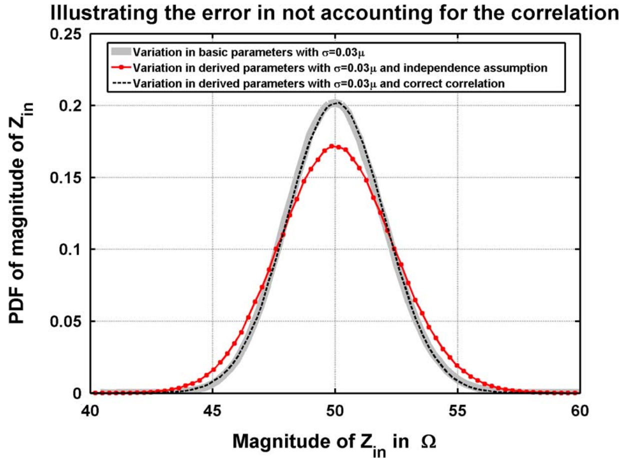


Fig. 2. Error in the PDF for a linear model of the objective function.

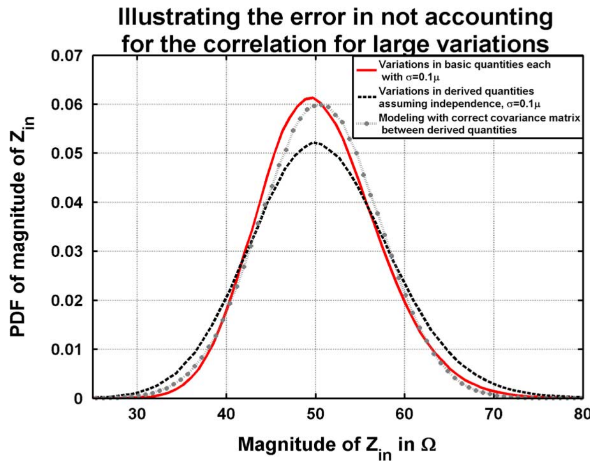


Fig. 3. Error in the PDF for a nonlinear model of the objective function.

the mean for all the parameters. It can be seen that, in this case, modeling through the derived variations by putting in the correct covariance matrix also yields a deviation in the PDF profile from the correct case. This is because the correlation coefficient accounts only for the linear dependence between two random variables, while larger process variations lead to nonlinear relationships with the basic process parameters.

The following observations can be made by considering the above two graphs. In the first case, the process variations are small. It can be shown by regression fit that the following linear relationships hold over the range of basic process parameters considered. As an example, for (2), the maximum error is 0.22% and the mean error is 0.05%. Equation (3) expresses the desired objective function in terms of the basic random variables, which are independent and Gaussian. Equation (4) expresses the desired objective function in terms of the derived random variables, which are jointly Gaussian for this case as follows:

$$Z_0 = -18.4918W - 9.9201\epsilon_r + 107.1319 \quad (1)$$

$$\beta = 0.4847W + 0.0109\epsilon_r + 0.1107 \quad (2)$$

$$|Z_{\text{in}}| = -28.0659W - 15.3133\epsilon_r + 137.6809 \quad (3)$$

$$|Z_{\text{in}}| = 1.5448Z_0 + 1.0318\beta - 28.3869. \quad (4)$$

Equation (3) expresses the required objective function in terms of the basic process variations, while (4) does the same in terms of the derived variations. The mapping onto the final objective function space from the basic variables space or the derived variables space will be exact. Knowing the PDFs of $W$ and $\epsilon_r$, the mean vector and the covariance matrix for the random vector $(Z_0, \beta)$ can be easily calculated. Since the relationships are linear, this defines an exact (almost within the small regression error) bivariate Gaussian PDF for $(Z_0, \beta)$. Hence, it is possible to determine the PDF of the desired objective function through derived variables alone [in this example, through (4)].

For the other case of larger process variations, the error in modeling through linear regression is large (mean error in $Z_0$ is 9.91%). Quadratic response surface yields errors below 1%. The relationships between the derived quantities and the basic process parameters are no longer linear. To uniquely determine the PDF of such derived quantities, it is necessary to specify more than the first two moments [15]. Thus, the mapping onto the final objective function from the derived variables space will be incorrect. Therefore, the PDF and the measures derived from them such as yield will be inaccurate. The same facts are true for the circuit equivalent parameters of electromagnetically modeled on-chip passive components.

### *B. Statistical Performance Analysis of Spiral Inductors*

This section focuses on the statistical study of on-chip spiral inductor performance using a full-wave field solver based on the Pogio–Miller–Chang–Harrington–Wu–Tsai (PMCHWT) formulation discussed extensively in [16]. Spiral inductors assume paramount importance in the design of many critical blocks such as low-noise amplifiers (LNAs), transformers, delay lines, and voltage-controlled oscillators. As analog and RF technologies progressively scale downwards, process variations directly impact spiral inductor performance.

Three independent variables have been selected for the statistical analysis of spiral inductors in this work; the track width of the metal layer in which the inductor is fabricated, the oxide thickness, and the substrate conductivity—all following Gaussian statistics. Details on the inductor dimensions and the response surface accuracy can be found in [11]. It is also shown in [11] that the PDFs of the derived variables such as the series inductance and series resistance assume non-Gaussian nature for larger process variations.

Results for the series inductance ($L$) for two types of variations are presented in Fig. 4.

It is noticeable that the obtained PDF for the extracted inductance $L$ is non-Gaussian for larger variations. To confirm this, the skewness of the PDFs for $L$ and $R$ are calculated. The skewness of a PDF (which is a measure of the non-Gaussian nature of the PDF), $\kappa$, is defined as follows [5]:

$$\kappa = \frac{E[(X-\mu)^3]}{\sigma^3}. \quad (5)$$

For the 5% input standard deviation, the skewness of $L$ and $R$ are 0.28 and 0.25, respectively. For the 10% input standard deviation, these are 0.55 and 0.48, respectively, depicting the

Authorized licensed use limited to: University of Washington Libraries. Downloaded on July 13, 2009 at 15:12 from IEEE Xplore. Restrictions apply.

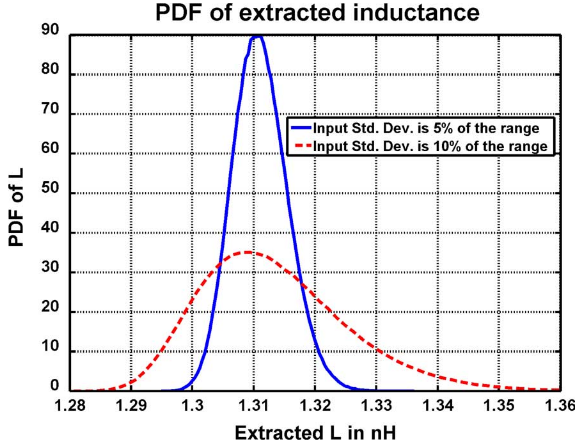


Fig. 4. PDF of extracted inductance (from [11]).

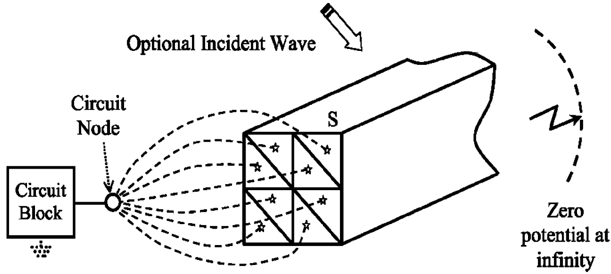


Fig. 5. General coupled circuit-EM system.

non-Gaussian nature of these PDFs. These two derived variables $L$ and $R$ are also correlated since they both depend on the same independent parameters through different functional forms (e.g., both $L$ and $R$ depend on the track width $W$).

## III. Statistical Analysis Methodology

### A. Statistical Coupled Circuit-EM Formulation

Consider a general system where the circuit part (modeled by a SPICE-like circuit solver) and the EM part (modeled by a full-wave EM field solver) are coupled through contacts as shown in Fig. 5. The EM surface is divided into two subsurfaces $S_{\rm EM}$ and $S_{\rm CK}$ to define the contacts. The details are presented in [17].

The system equations can be written as follows, with $\mathbf{MNA}$ and $\mathrm{EM}$ denoting single variables that represent matrices in the discussion to follow:

$$\begin{bmatrix} \mathbf{Z_{11}} & \mathbf{Z_{12}} & \mathbf{0} \\ \mathbf{Z_{21}} & \mathbf{Z_{22}} & \mathbf{C} \\ \mathbf{0} & \mathbf{C^T} & \mathbf{MNA} \end{bmatrix} \begin{bmatrix} \mathbf{i} \\ \mathbf{j_c} \\ \mathbf{ckt} \end{bmatrix} = \begin{bmatrix} \mathbf{v_{em}} \\ \mathbf{0} \\ \mathbf{v_{ckt}} \end{bmatrix} \tag{6}$$

where $\mathbf{Z_{11}}$ is the usual method of moments (MoM) matrix whose elements can be interpreted as the equivalent partial impedances. $\mathbf{Z_{12}}$ denotes the scalar potential contribution due the coupling current at $S_{\rm EM}$, $\mathbf{Z_{21}}$ denotes the potential contribution from the EM surface current at $S_{\rm CK}$. Finally, the matrix $\mathbf{Z_{22}}$ represents the scalar potential contribution to $S_{\rm CK}$ due to the coupling current. A sparse rectangular matrix $C$ is introduced as connection matrix to enforce the generalized Kirchoff's current law and Kirchoff's voltage law. This two-by-two system is a self-consistent definition of the EM interactions with a circuit section. To complete the coupled formulation, a sparse rectangular matrix is introduced as connection matrix to enforce generalized Kirchoff's current law and Kirchoff's voltage law. This matrix has one nonzero element per row to select the potential of the circuit node associated with a contact triangle. The transpose matrix selects the coupling current and adds it to the Kirchoff's current law equation of the circuit node at the contact. The modified nodal analysis (MNA) matrix represents circuit interactions for linear *RLC* elements and the linearized small-signal models of nonlinear elements such as diodes and transistors. The system unknowns $\mathbf{i}$, $\mathbf{j_c}$, and $\mathbf{ckt}$ relate to surface equivalent currents, coupling currents, and circuit voltages and currents, respectively. The right-hand-side excitation vector consists of the tested incident EM field, the strengths of independent voltage, and current sources [18].

In the presence of process variations, the matrix elements become random entries, depending on the process parameters. Let $\bar{\alpha}$ represent the vector of process parameters affecting the circuit part and $\bar{\beta}$ represent the vector of process parameters affecting the EM part. The above equation is then modified as

$$\begin{bmatrix} \mathbf{Z_{11}}(\bar{\boldsymbol{\beta}}) & \mathbf{Z_{12}}(\bar{\boldsymbol{\beta}}) & \mathbf{0} \\ \mathbf{Z_{21}}(\bar{\boldsymbol{\beta}}) & \mathbf{Z_{22}}(\bar{\boldsymbol{\beta}}) & \mathbf{C} \\ \mathbf{0} & \mathbf{C^T} & \mathbf{MNA}(\bar{\boldsymbol{\alpha}}) \end{bmatrix} \begin{bmatrix} \mathbf{i}(\bar{\boldsymbol{\alpha}},\bar{\boldsymbol{\beta}}) \\ \mathbf{j_c}(\bar{\boldsymbol{\alpha}},\bar{\boldsymbol{\beta}}) \\ \mathbf{ckt}(\bar{\boldsymbol{\alpha}},\bar{\boldsymbol{\beta}}) \end{bmatrix} = \begin{bmatrix} \mathbf{v_{em}} \\ \mathbf{0} \\ \mathbf{v_{ckt}} \end{bmatrix}. \tag{7}$$

The eventual objective functions (gain or return loss of an RF amplifier) needed are functions of the excitation $\mathbf{v_{ckt}}$ (assuming that the EM excitation is zero—signifying that the EM elements are used as passive elements and that there is no external radiation) and the currents $\mathbf{i}$, $\mathbf{j_c}$, and $\mathbf{ckt}$. One way to solve this problem would be to express all the matrix elements in (7) as functions of the parameters in the process parameter vectors $\boldsymbol{\alpha}$ and $\boldsymbol{\beta}$, and obtain a symbolic inverse for the matrix and then solve for the objective function desired. The PDF of the objective function can then be determined from such a relation. It can be easily seen that this method is not feasible beyond very small matrices. Hence, a port-model-based approach is used to circumvent this difficulty.

The port model is a widely used approach for circuit designers to include EM effects. In addition to being used as a fully coupled solver, the formulation presented in [17] can also be used in a manner similar to port-model approaches. Equation (7) can be recast in the following form:

$$\begin{bmatrix} \mathbf{EM}(\bar{\boldsymbol{\beta}}) & \mathbf{C}' \\ \mathbf{C'^T} & \mathbf{MNA}(\bar{\boldsymbol{\alpha}}) \end{bmatrix} \begin{bmatrix} \mathbf{i}'(\bar{\boldsymbol{\alpha}},\bar{\boldsymbol{\beta}}) \\ \mathbf{ckt}(\bar{\boldsymbol{\alpha}},\bar{\boldsymbol{\beta}}) \end{bmatrix} = \begin{bmatrix} \mathbf{v}'_{\mathbf{em}} \\ \mathbf{v_{ckt}} \end{bmatrix} \tag{8}$$

where $\mathbf{EM}$ contains the matrices, $\mathbf{Z_{11}}, \mathbf{Z_{12}}, \mathbf{Z_{21}}$, and $\mathbf{Z_{22}}$ from (6). $\mathbf{C}'$, $\mathbf{i}'$, and $\mathbf{v}'_{\mathbf{em}}$ are the extensions of their corresponding entry in (6). In (8), letting $\mathbf{v}'_{\mathbf{em}} = 0$, the coupling current unknowns $\mathbf{i}'$ can be eliminated from the first set of equations and

Authorized licensed use limited to: University of Washington Libraries. Downloaded on July 13, 2009 at 15:12 from IEEE Xplore. Restrictions apply.

the rest of the system can be written in Schur complement form as

$$(\mathbf{MNA}(\bar{\boldsymbol{\alpha}}) - \mathbf{C}'^{\mathbf{T}}\mathbf{EM}(\bar{\boldsymbol{\beta}})^{-1}\mathbf{C}')\mathbf{ckt}(\bar{\boldsymbol{\alpha}},\bar{\boldsymbol{\beta}}) = \mathbf{v_{ckt}} \quad (9)$$

where it is assumed that there is no external excitation to the EM part of the system such as an incident wave. The term $\mathbf{C}'^{\mathbf{T}}\mathbf{EM}(\bar{\boldsymbol{\alpha}},\bar{\boldsymbol{\beta}})^{-1}\mathbf{C}'$, therefore, parameterizes the EM object. Thus, it facilitates replacing of the EM object by a port-based network parameter such as the $y$-parameter used in this paper. This will inherently capture all the full-wave effects and permit a highly accurate analysis of the coupled circuit-EM system. The dependence on the process parameters $\bar{\alpha}, \bar{\beta}$ are captured through deterministic sampling through the response surface models. Port calibration is an important issue and if the port impedance differs from the nominal value of 50 Ω in a statistical fashion that can introduce errors in the PDF. It is pronounced with the usage of "wave ports," which are common in some commercial simulators. In this particular work, the solver is based on a coupled EM-circuit formulation in [17], which models the electrically small ports as measurement points. These are more appropriate sources for modeling the behavior of passive elements in an RF circuit environment.

### *B. y-Parameter-Based Combined Circuit-EM Statistical Analysis Method*

The proposed methodology for statistical analysis of coupled circuit-EM systems relies on the flow summarized in Fig. 6. The sources of variation in the circuit part and associated EM objects are identified *a priori*. The circuit and EM parts are decoupled at the points where the EM objects connect to the circuits, thus defining ports. Steps 1 and 2 compute the $y$-parameters for the circuit and EM parts. Steps 3 and 4 generate response surfaces. Steps 5 and 6 compute the $y$-parameters of the circuit and EM parts, which are required in the rapid Monte Carlo analysis, while step 7 combines the $y$-parameters and computes the desired objective function. The output of step 7 is used to bin the samples and to furnish the PDFs of the overall circuit performance measures.

Casting these details in algebraic form will clarify this even further. Let $G$ represent a high-level circuit performance measure, for example, the gain of an LNA. Let $y_{i\mathrm{cir}}, i = 1$ to $N_{\mathrm{cir}}$ and $y_{j\mathrm{em}}, j = 1$ to $N_{\mathrm{em}}$ represent the $y$-parameters of the circuit part and the EM parts, respectively. From network theory, it is possible to write the general form of a desired objective function $G$, which is a terminal quantity such as gain, return loss, input, or output impedance as

$$G = \frac{f_1(y_{1\mathrm{cir}}, y_{2\mathrm{cir}} \cdots, y_{1\mathrm{em}}, y_{2\mathrm{em}}, \cdots)}{f_2(y_{1\mathrm{cir}}, y_{2\mathrm{cir}} \cdots, y_{1\mathrm{em}}, y_{2\mathrm{em}}, \cdots)}. \quad (10)$$

Here, $f_1$ and $f_2$ are functions involving one or more of the circuit and EM $y$-parameters. Their general form is that of polynomials in multiple variables. This is illustrated by the (18) in Section III-C. In this case,

$$f_1 = (y_{\mathrm{cir}} + y_{22t}) \quad (11)$$

$$f_2 = (y_{11t}y_{\mathrm{cir}} + (y_{11t}y_{22t} - y_{12t}y_{21t})). \quad (12)$$

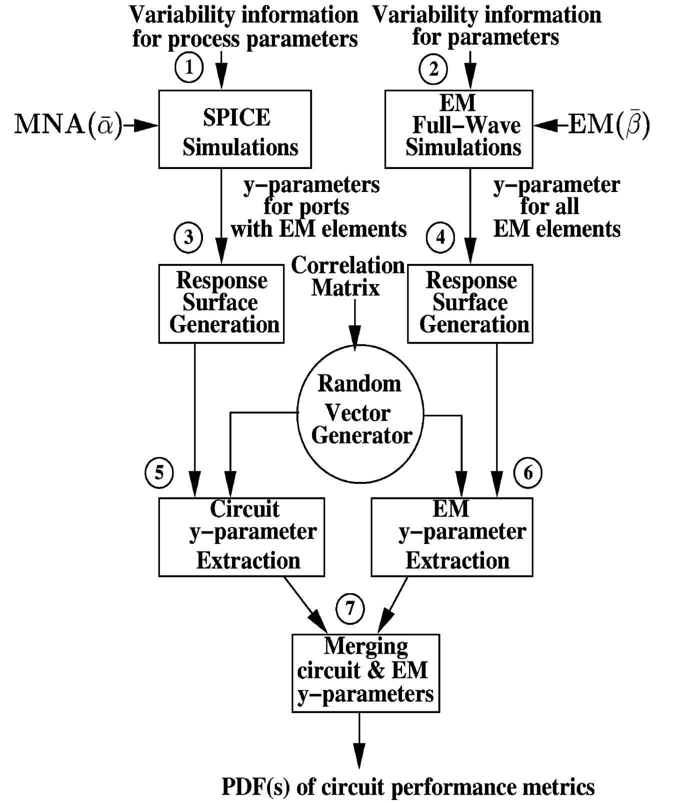


Fig. 6. Flow to extract PDF of circuit performance metrics.

Again, each of these $y$-parameters are expressible as response surface models of the underlying Gaussian random variables, which represent the process variations. Thus, in a hierarchical manner, the eventual performance measure can be expressed as

$$G = \frac{g_1(p_{1\mathrm{cir}}, p_{2\mathrm{cir}} \cdots, p_{1\mathrm{em}}, p_{2\mathrm{em}}, \cdots)}{g_2(p_{1\mathrm{cir}}, p_{2\mathrm{cir}} \cdots, p_{1\mathrm{em}}, p_{2\mathrm{em}}, \cdots)} \quad (13)$$

where $p_{1\mathrm{cir}}$, $p_{1\mathrm{em}}, \ldots,$ represent the basic process-dependent parameters for the device and the EM structures. It is to be noted that while (10) is exact, (13) is approximate, owing to regression errors. They can be minimized by constructing higher order models for the $y$-parameters in terms of the basic process variables. Expressing the $y$-parameters in terms of the input variables requires constructing the response surface. RSM is a very popular interpolation method used in many branches of engineering [19]. Methods such as space mapping [20] and artificial neural networks [21] are also very effective in providing this kind of a nonlinear mapping from the input process parameters and the $y$-parameters. The RSM approach is undertaken owing to the simplicity of the implementation and sufficiency of the accuracy for statistical analysis.

If the objective function $y$ depends on a vector of input variables $[x_1, x_2, \ldots, x_n]$, a quadratic or second-order response for $y$ in terms of the input variables implies that $y$ is expressible as

$$y = a_0 + \mathbf{a}^T\mathbf{x} + \mathbf{x}^T\mathbf{B}\mathbf{x} \quad (14)$$

where $\mathbf{x}$ is the $n$ column vector of the input variables, $\mathbf{a}$ is the $n$ column vector of the linear term coefficients, and $\mathbf{B}$ is the $n \times n$ matrix for the coefficients of the nonlinear terms. Let

Authorized licensed use limited to: University of Washington Libraries. Downloaded on July 13, 2009 at 15:12 from IEEE Xplore. Restrictions apply.

there be $m$ evaluations of the objective function. For a linear response surface, the coefficients are determined by minimizing the least square error of a typically overdetermined system by the solution to the equation

$$\mathbf{A} = (\mathbf{X}^T\mathbf{X})^{-1}\mathbf{X}^T\mathbf{v} \tag{15}$$

where $\mathbf{X}$ is the matrix of size $m \times (n+1)$ where the first column is all 1's and the remaining entries are formed from the values of the input variables $x_i$ corresponding to the particular objective function evaluation. The vector $\mathbf{v}$ is comprised of the observed values of the objective function. The second-order response surface is constructed similarly by introducing new variables for the square and cross terms.

The idea is to capture the eventual objective function in terms of the basic process parameters to facilitate the sampling process. They may or may not exhibit Gaussian statistics. Gaussian assumption is used in this paper because of its ubiquitous usage. Methods exist to generate samples from independent non-Gaussian PDFs [15].

The usage of the $y$-parameter approach provides seamless integration between EM and circuit modeling strategies while addressing all the issues mentioned in Section I.

### C. Proposed Methodology Applied to a Transmission Line

In this section, the same transmission line paradigm is used to illustrate the proposed methodology. Let the transmission line be taken as the electromagnetically modeled system (though it is modeled through empirical equations as pointed out in Section II-A). The transmission line is terminated by a load resistance $(Z_l)$ of 50 $\Omega$, which is taken to be the circuit part. The $y$-parameters (it is possible to use other network parameters too) of the transmission line are given as

$$y_{11} = y_{22} = \frac{\coth(\gamma l)}{Z_0} \tag{16}$$

$$y_{12} = y_{21} = \frac{\operatorname{cosech}(\gamma l)}{Z_0} \tag{17}$$

where $\gamma$ denotes the complex propagation constant and $l$ denotes the length of the transmission line. In the case of the actual coupled circuit-EM systems, these $y$-parameters are available as outputs from the field solver. The $y$-parameter of the circuit part $(y_{\text{cir}})$ is just $(1/Z_l)$. The objective function of interest, namely, $|Z_{\text{in}}|$, can then be computed using the relationship obtained from simple network theory as

$$Z_{\text{in}} = \frac{\left(1 + y_{22t}\left(\frac{1}{y_{\text{cir}}}\right)\right)}{\left(y_{11t} + (y_{11t}y_{22t} - y_{12t}y_{21t})\left(\frac{1}{y_{\text{cir}}}\right)\right)}. \tag{18}$$

The subscript $t$ refers to the transmission line and the subscript $\text{cir}$ refers to the circuit part, which is just a load resistance in this example. In order to capture the eventual objective functions in terms of the basic process variables, it is necessary to express the $y$-parameters of the transmission line part and the circuit part in terms of their corresponding basic variables representing the process variations using response surfaces.

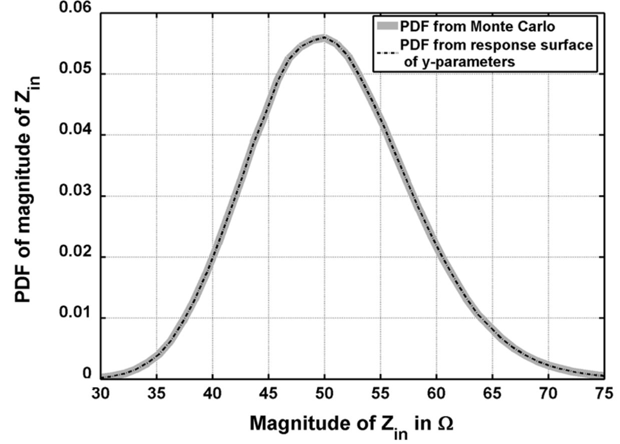


Fig. 7. Comparison of the Monte Carlo method with analytical model with the response surface-based $y$-parameter technique.

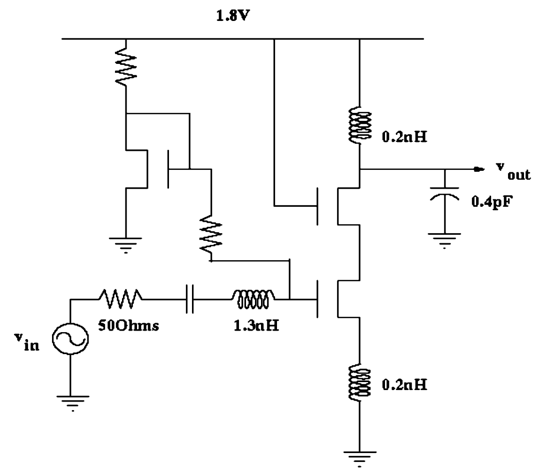


Fig. 8. Single-ended RF amplifier schematic.

Quadratic modeling is used to express the $y$-parameters of the transmission line in terms of its basic process variations, namely, $W$ and $\epsilon_r$. The circuit part in this particular case does not need any response surface modeling.

Fig. 7 compares the PDFs obtained from Monte Carlo analysis and the proposed methodology for the case where the standard deviation is a fraction 0.1 of the mean. The two curves completely overlap. This verifies the proposed decoupled terminal parameter-based method by a direct comparison with the Monte Carlo method.

## IV. RF Amplifiers

### A. Single-Ended RF Amplifier

The proposed methodology has been applied to the statistical analysis of performance metrics of a single-ended RF amplifier shown in Fig. 8 [22]. The circuit represents an RF amplifier designed in a 0.18-$\mu$m RF CMOS process with a center frequency $(f_c)$ of 15.78 GHz and a bandwidth of 900 MHz. The voltage gain in the absence of process variations is 17 dB. The minimum achievable noise figure is 1.92 dB. In this paper, random variations in gate–oxide thickness, zero body-bias threshold voltage,

Authorized licensed use limited to: University of Washington Libraries. Downloaded on July 13, 2009 at 15:12 from IEEE Xplore. Restrictions apply.

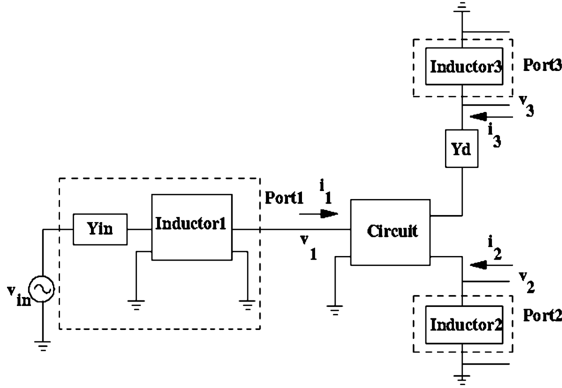


Fig. 9. $y$-parameter port definitions for the single-ended RF amplifier circuit.

and reduction in channel length have been taken into account. The dependence of zero body-bias threshold voltage on oxide thickness is captured using correlation between these BSIMv3 SPICE MOSFET model parameters. Intra-die variations have not been taken into account in this paper.

An automated flow has been developed to extract all the necessary $y$-parameters of circuit without the EM objects with Fig. 8 being one such example. A black box approach inherent in $y$-parameter extraction automatically encapsulates all the intrinsic parasitics of the MOS transistors.

Response surfaces are constructed for each of the $y$-parameters by means of a three-variable full factorial design.

The interconnection between the circuit and three inductors for the aforementioned circuit is outlined in Fig. 9. There are four sets of $y$-parameters, one belonging to the circuit and the other three belonging to the inductors, respectively. The circuit $y$-parameters are identified by the superscript $c$, while the $y$-parameters of the three inductors are superscripted by $1L, 2L$, and $3L$, respectively. For Inductor1, the $y$-parameters are inclusive of the source admittance $Y_{\text{in}}$ in Fig. 9. The system of linear equations that need to be solved in order to calculate all the node voltages of the circuit can be expressed in matrix form as

$$\begin{bmatrix} y_{11}^c + y_{22}^{1L} & y_{12}^c & y_{13}^c \\ y_{21}^c & y_{22}^c + y_{11}^{2L} & y_{23}^c \\ y_{31}^c & y_{32}^c & y_{33}^c + y_{11}^{3L} \end{bmatrix} \begin{bmatrix} v_1 \\ v_2 \\ v_3 \end{bmatrix} = \begin{bmatrix} -y_{21}^{1L} v_{\text{in}} \\ 0 \\ 0 \end{bmatrix} \tag{19}$$

$$\text{Gain} = \frac{v_3}{v_{\text{in}}} = \frac{-y_{21}^{1L}\left(y_{21}^c y_{32}^c - y_{31}^c y_{22}^c - y_{31}^c y_{11}^{2L}\right)}{\Delta}. \tag{20}$$

The term $\Delta$ represents the determinant of the matrix involving circuit and EM $y$-parameters. Similarly, quantities like input and output impedance and input reflection coefficient are calculated by using closed-form expressions in terms of both circuit and EM $y$-parameters. Random samples are generated for the basic independent process parameters. The corresponding realizations of circuit and EM $y$-parameters are then computed using the various response surface relations. The final objective functions are evaluated from the $y$-parameter relations such as the one in (20).

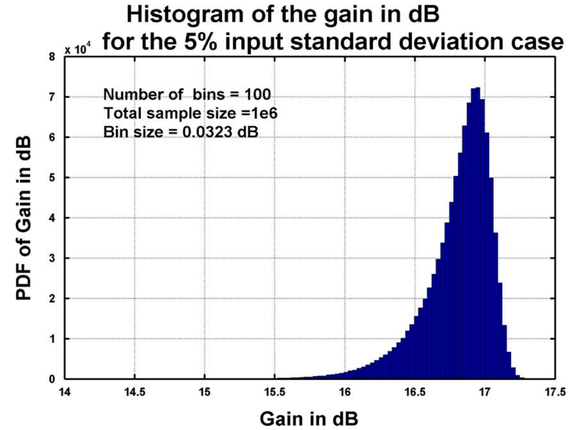


Fig. 10. PDF of the gain for input standard deviation of 10% of the range.

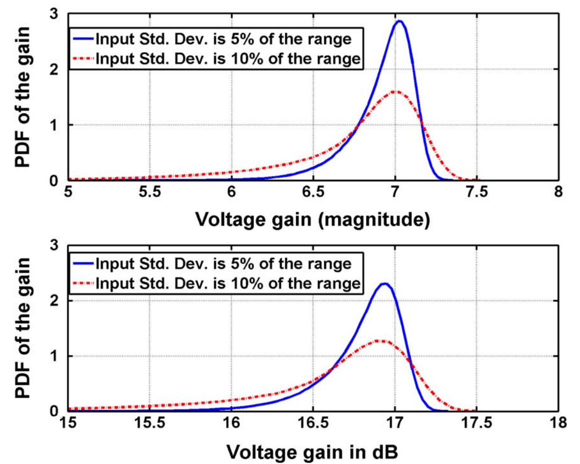


Fig. 11. PDF of the gain for two different variations at $f_c$ (from [11]).

The authors in [23] propose an automated technique to combine two subcircuits characterized by their transfer functions, utilizing a general interconnection template for outlining connectivity between the subcircuits. The transfer function of smaller subcircuits are then combined in sequence to generate transfer functions for larger circuits.

Results are now presented for the circuit performance measures. For the 5% input standard deviation variation, the PDF is shown in Fig. 10 as binned results from the Monte Carlo analysis on the gain expression discussed in (20). The number of bins is 100 giving a bin size of 0.0323 dB. Subsequent PDFs are shown as continuous curves obtained by connecting the mid points of the bins.

Fig. 11 represents the PDF of the gain for two different types of variations—standard deviation of 5% and standard deviation of 10% of the total range considered for all the varying parameters, respectively. PDFs for the absolute value of the voltage gain and the gain in decibels are shown and both are observed to be skewed. This emphasizes the fact that the skewness is not arising due to expressing the gain in decibels. An interesting observation is that the gain mostly worsens from the mean design in the presence of process variations, and this effect is enhanced by taking into account the variability in the EM objects. This is attributed to the fact that any process variation will tune the

Authorized licensed use limited to: University of Washington Libraries. Downloaded on July 13, 2009 at 15:12 from IEEE Xplore. Restrictions apply.

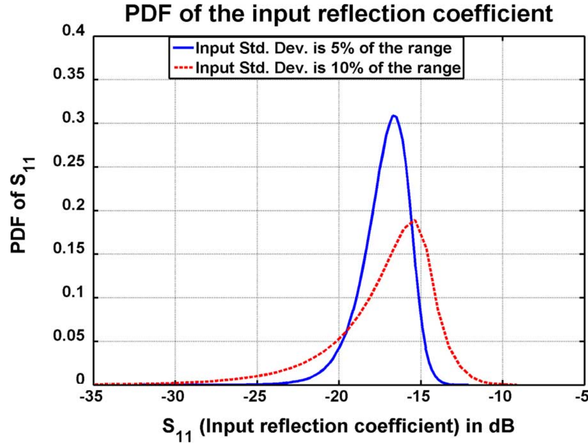


Fig. 12. PDF of the $S_{11}$ in decibels for two different variations at $f_c$ (from [11]).

TABLE I
SKEWNESS FOR THE DIFFERENT PDFs OF RF AMPLIFIER PERFORMANCE

| Amplifier performance | Input $\sigma$=0.05Range | Input $\sigma$=0.1Range |
|---|---|---|
| Gain | -1.51 | -2.14 |
| $S_{11}$ | -0.94 | -1.73 |
| $Z_{out}$ | -1.73 | -2.10 |

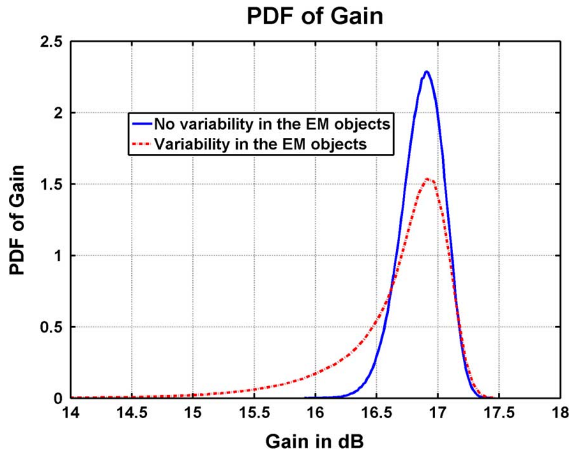


Fig. 13. Effect of EM variability on the PDF of gain at $f_c$ (from [11]).

amplifier away from the designed center frequency thereby incurring a loss in gain at that frequency.

Fig. 12 depicts the PDFs for the input reflection coefficient for the same two types of variations. A calculation of the skewness is undertaken for all the PDFs and are summarized in Table I. Kurtosis of a PDF is defined as its the fourth central moment. The kurtosis values for these PDFs range from 4.9 to 9.5, depicting a significant deviation from the kurtosis of a Gaussian PDF that has a value of 3.

Next, the statistical analysis is done without and with the variability in the EM modeled objects. It can be seen in Fig. 13 that variability in EM objects affects the PDF of the gain significantly. The circuit variability has been kept the same in both cases. All variations are 10% input standard deviation, as explained previously.

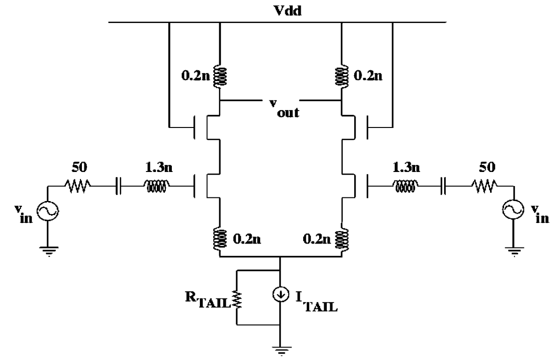


Fig. 14. Differential RF amplifier schematic.

### B. Differential RF Amplifier

The proposed methodology has also been applied to the statistical analysis of performance metrics of a topologically symmetrical differential RF amplifier shown in Fig. 14 working at the same frequency as the single-ended RF amplifier considered earlier. This example has been studied in detail in [24]. The $I_{\mathrm{TAIL}}$ is chosen such that the $g_m$ of the transistors remain the same, thus providing a differential gain of 17 dB [25]. The differential pair is partitioned into two halves—left and right—and the process parameters are assumed to be perfectly correlated between the transistors within the respective halves. A correlation coefficient of 0.8 has been assumed between the pairs of similar parameters across the two halves. It is to be noted that the response surfaces for the $y$-parameters are built for the half circuit once only. The final objective functions are then expressed in terms of two sets of circuit and EM $y$-parameters for the left and right halves to model the mismatch. The samples for the two sets of $y$-parameters are then generated from these models, while preserving the correlation between the process parameters for the two halves. This approach facilitates reusability without sacrificing accuracy.

Using network analysis, the quantities like differential gain, input and output impedances, the differential return loss, and the common mode rejection ratio, can all be expressed in terms of the $y$-parameters of the blocks similar to Fig. 9. Results are presented for the PDFs of the differential gain and differential return loss in Figs. 15 and 16, respectively.

The PDF in Fig. 15 appears choppy towards the larger values of the gain. This can be explained as follows. Due to process variations, the center frequency of the amplifier moves away from the designed $f_c$. Hence, the gain is lowered at the original center frequency at which the study is made. A result of this is the number of samples beyond the nominal gain decreasing dramatically. Therefore, maintaining the same bin size will yield a choppy PDF. If the bin size is increased for gain beyond the nominal value, again the PDF appears choppy because of the larger spacing between the bins. Hence, the noisy PDF appearance in this figure has a physical origin. The noise appearing in Fig. 16 is numerical noise, which can be eliminated by using more samples and correspondingly smaller bin sizes.

Authorized licensed use limited to: University of Washington Libraries. Downloaded on July 13, 2009 at 15:12 from IEEE Xplore. Restrictions apply.

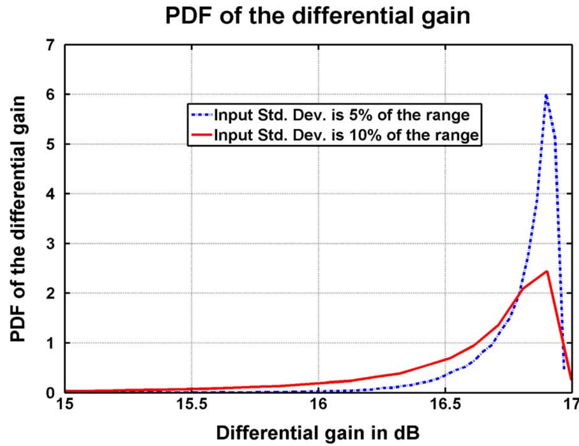


Fig. 15. PDF of the differential gain for two types of variation (from [24]).

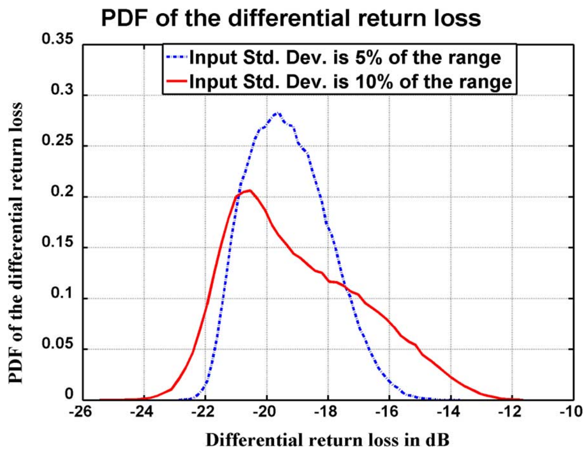


Fig. 16. PDF of the differential return loss for two types of variation (from [24]).

## V. Yield Computation

Let $\mathbf{p} = [p_1, p_2 \ldots\ldots, p_n]$ represent the vector of various desired performance measures that are needed to qualify the yield measure. Let $C$ denote the hypercube in $n$ dimensions that encloses the range of all these performance measures. This is defined by the limits of performance measures for each of the performance measures, whereby $p_{i_{\min}} \leq p_i \leq p_{i_{\max}}$. Let the joint PDF of the $n$ performance measures be $f_{\mathbf{P}}(\mathbf{p})$. The yield measure $Y$ is then the integral

$$Y = \int_{p_{1_{\min}}}^{p_{1_{\max}}} \cdots \int_{p_{n_{\min}}}^{p_{n_{\max}}} f_{P_1,\ldots P_n}(p_1, \ldots p_n) dp_1 \ldots dp_n \tag{21}$$

$$= \int_C f_{\mathbf{P}}(\mathbf{p}) d\mathbf{p}. \tag{22}$$

The integral in (21) can be computed in a Monte Carlo fashion from the samples for the performance measures, which are generated from the closed-form expressions similar to (13). This has been applied to two different scenarios.

- On-chip inductor: Here, the inductor connected to the drain of the MOSFET in Fig. 8 is taken as an example. The mean inductance is 0.2079 nH and the mean quality factor ($Q$) is 16.8. Under process variations, if the inductance is required to be within 5% range of the mean and if the desired $Q$ factor is to be at least 15, the yield can be computed to be 91.5%. The yield diagram is shown in Fig. 17. This is a scatter diagram showing $L$ and $Q$ under process variations. The good inductors (the ones that satisfy the yield criteria) are plotted in the darker shade, while the lighter shade represents all the inductors.
- Single-ended RF amplifier of Section IV-A. Table II summarizes the yields for different criteria of performance parameters of the single-ended RF amplifier discussed in order to demonstrate the effect of process variations.
  The yield diagram is shown below in Fig. 18 for a 10% input standard deviation.

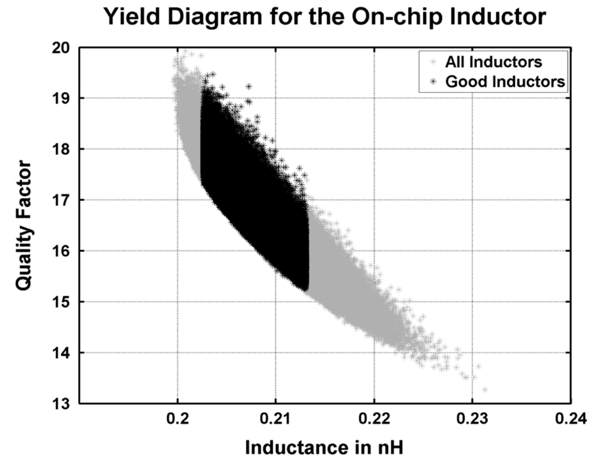


Fig. 17. Yield diagram for 10% input standard deviation for the on-chip inductor.

TABLE II
Yield Table (From [11])

| Circuit Performance | Input $\sigma$=0.05Range | Input $\sigma$=0.1Range |
|---|---|---|
| Gain $>$ 16 dB | 89.28% | 70.45% |
| $S_{11}$ $<$ -15 dB | 96.58% | 77.85% |
| Overall | 86.23% | 50.06% |

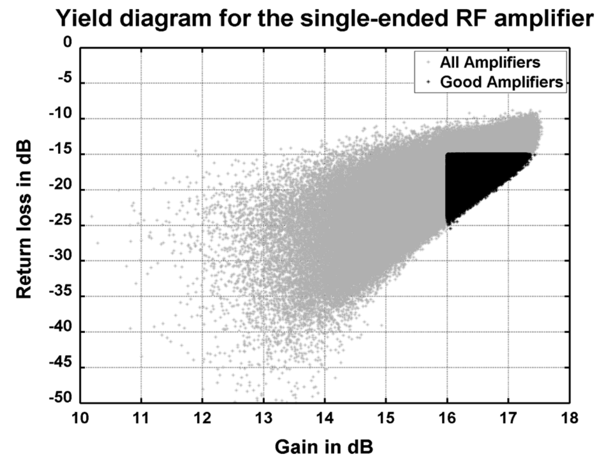


Fig. 18. Yield diagram for 10% input standard deviation for the single-ended RF amplifier.

Authorized licensed use limited to: University of Washington Libraries. Downloaded on July 13, 2009 at 15:12 from IEEE Xplore. Restrictions apply.

## VI. Conclusion

This paper has proposed a hierarchical methodology for statistical analysis of RF circuits with the passive elements modeled by a full-wave EM solver. Employing circuit models for these passive elements for statistical analysis using SPICE-like circuit simulators presents some challenges. These issues are illustrated by using a simple transmission line analogy. It is shown by the statistical analysis of the on-chip spiral inductors that the same issues are true for the passive elements modeled by a field solver. To circumvent these issues, a technique based on decoupled terminal parameters has been proposed. The eventual objective functions are captured in terms of the independent basic process parameters. This facilitates a rapid Monte Carlo analysis on the closed-form expressions in order to obtain the desired PDFs. This further enables calculation of yield measures based on criteria for multiple objective functions. An automated flow has been developed to do the statistical analysis on different performance parameters of an RF amplifier and its differential version.

Future work will focus on hierarchical and adaptive response surface generation to minimize the number of calls to the field-solver library-based methods to expedite the PDF extraction and the application of the proposed methodology to larger-scale subsystems through multilevel hierarchical methods. Usage of rational polynomial fitting techniques for $S$-parameters, such as asymptotic waveform evaluation, in conjunction with a fast full-wave solver enables generation of accurate time-domain response using the robustness of spectral-domain solvers. It is proposed that these techniques be used to generate PDFs of time-domain-based objective functions of coupled circuit EM systems.

## References


[1] S. R. Nassif, "Modeling and analysis of manufacturing variations," in *IEEE Custom Integr. Circuits Conf.*, 2001, pp. 223–238.

[2] S. Zanella, A. Nardi, A. Neviani, M. Quarantelli, S. Saxena, and C. Guardiani, "Analysis of the impact of process variations on clock skew," *IEEE Trans. Semiconduct. Manuf.*, vol. 13, no. 4, pp. 401–407, Nov. 2000.

[3] A. Agarwal, D. Blaauw, and V. Zolotov, "Statistical timing analysis for intra-die process variations with spatial correlations," in *IEEE/ACM Int. Comput.-Aided Design Conf.*, 2003, pp. 900–907.

[4] J. Wang, P. Ghanta, and S. Vrudhula, "Stochastic analysis of interconnect performance in the presence of process variations," in *IEEE/ACM Int. Comput.-Aided Design Conf.*, 2004, pp. 880–886.

[5] S. Abbaspour, H. Fatemi, and M. Pedram, "Non-Gaussian statistical interconnect timing analysis," in *Design, Automat., Test in Eur.*, 2006, pp. 533–538.

[6] E. Felt, S. Zanella, C. Guardiani, and A. Sangiovanni-Vincentelli, "Hierarchical statistical characterization of mixed-signal circuits using behavioral modeling," in *IEEE/ACM Int. Comput.-Aided Design Conf.*, 1996, pp. 374–380.

[7] A. A. Mutlu and M. Rahman, "Statistical methods for the estimation of process variation effects on circuit operation," *IEEE Trans. Electron. Packag. Manuf.*, vol. 28, no. 4, pp. 364–375, Oct. 2005.

[8] X. Li, J. Le, P. Gopalakrishnan, and L. T. Pileggi, "Asymptotic probability extraction for non-normal distributions of circuit performance," in *IEEE/ACM Int. Comput.-Aided Design Conf.*, 2004, pp. 2–9.

[9] E. Matoglu, N. Pham, D. N. de Araujo, M. Cases, and M. Swaminathan, "Statistical signal integrity analysis and diagnosis methodology for high-speed systems," *IEEE Trans. Adv. Packag.*, vol. 27, no. 4, pp. 611–629, Nov. 2004.

[10] S. Mukherjee, M. Swaminathan, and E. Matoglu, "Statistical analysis and diagnosis methodology for RF circuits in LCP substrates," *IEEE Trans. Microw. Theory Techniques*, vol. 53, no. 11, pp. 3621–3630, Nov. 2005.

[11] A. V. Sathanur, R. Chakraborty, and V. Jandhyala, "Statistical analysis of RF circuits using combined circuit simulator-full wave field solver approach," in *IEEE/ACM Int. Comput.-Aided Design Conf.*, 2007, pp. 11–17.

[12] J. Gil and H. Shin, "A simple wide-band on-chip inductor model for silicon-based RF ICs," *IEEE Trans. Microw. Theory Tech.*, vol. 51, no. 9, pp. 2023–2028, Sep. 2003.

[13] M. Kang, J. Gil, and H. Shin, "A simple parameter extraction method of spiral on-chip inductors," *IEEE Trans. Electron Devices*, vol. 52, no. 9, pp. 1976–1981, Sep. 2005.

[14] D. M. Pozar, *Microwave Engineering.*, 3rd ed. New York: Wiley, Jan. 2004.

[15] A. Papoulis and S. Pillai, *Probability, Random Variables and Stochastic Processes*. New York: McGraw-Hill, 2002.

[16] K. Umashankar, A. Taflove, and S. Rao, "Electromagnetic scattering by arbitrarily shaped three-dimensional homogeneous lossy dielectric objects," *IEEE Trans. Antennas Propag.*, vol. 34, no. 6, pp. 758–766, Jun. 1986.

[17] Y. Wang, D. Gope, V. Jandhyala, and C.-J. R. Shi, "Generalized Kirchoff's current and voltage law formulation for coupled circuit-electromagnetic simulation with surface integral equations," *IEEE Trans. Microw. Theory Tech.*, vol. 52, no. 7, pp. 1673–1682, Jul. 2004.

[18] J. Vlach and K. Singhal, *Computer Methods for Circuit Analysis and Design*. New York: Van Nostrand, 1983.

[19] R. H. Myers and D. C. Montgomery, *Response Surface Methodology: Process and Product Optimization Using Designed Experiments.*, 2nd ed. New York: Wiley, 2002.

[20] J. W. Bandler, R. M. Biernacki, S. H. Chen, P. A. Grobelny, and R. H. Hemmers, "Space mapping technique for electromagnetic optimization," *IEEE Trans. Microw. Theory Tech.*, vol. 42, no. 12, pp. 2536–2544, Dec. 1994.

[21] O. A. Mohammed, D. C. Park, F. G. Uler, and C. Ziqiang, "Design optimization of electromagnetic devices using artificial neural networks," *IEEE Trans. Magn.*, vol. 28, no. 5, pp. 2805–2807, Sep. 1992.

[22] T. H. Lee, *The Design of CMOS Radio-Frequency Integrated Circuits*. Cambridge, U.K.: Cambridge Univ. Press, 1998.

[23] M. Ranjan and R. Vemuri, "Exact hierarchical symbolic analysis of large analog networks using a general interconnection template," in *Int. Circuits Syst. Symp.*, 2006, pp. 1776–1779.

[24] A. V. Sathanur, R. Chakraborty, and V. Jandhyala, "Accurate statistical analysis of a differential low noise amplifier using a combined spice-field solver approach," in *Int. Circuits Syst. Symp.*, 2008, pp. 884–887.

[25] B. Razavi, *Design of Analog CMOS Integrated Circuits*. New York: McGraw-Hill, 2000.

**Arun V. Sathanur** (S'06) received the Masters degree in electrical communication engineering from the Indian Institute of Science (IISc), Bangalore, India, in 2005, and is currently working toward the Ph.D. degree at the University of Washington, Seattle.

He is currently with the Applied Computational Engineering Laboratory, Department of Electrical Engineering, University of Washington. During Summer 2007, he was an Intern with the Electrical Core Competency (ECC) Group, Intel Corporation, Chandler, AZ, where he was involved with optimization of high-speed microprocessor packages. His research interests include engineering optimization, statistical analysis, signal integrity, and high-speed package design.

Mr. Sathanur was the recipient of the 2008–2009 Intel Fellowship.

**Ritochit Chakraborty** received the Bachelors degree from the Birla Institute of Technology and Science (BITS), Pilani, India, in 2001, the Masters degree in computer engineering from the University of Cincinnati, Cincinnati, OH, in 2006, and is currently working toward the Ph.D. degree at the University of Washington, Seattle. His Masters thesis concerned analog design automation.

From 2001 to 2003, he was with the Set Top Box Design Group, STMicroelectronics, India. His research interests include analog and RF CAD, signal integrity, statistical analysis, and circuit simulation.

Authorized licensed use limited to: University of Washington Libraries. Downloaded on July 13, 2009 at 15:12 from IEEE Xplore. Restrictions apply.

**Vikram Jandhyala** (S'96–M'00–SM'03)received the B.Tech. degree in electrical engineering from the Indian Institute of Technology (IIT), Delhi, India, in 1993, and the M.S. and Ph.D. degrees from the University of Illinois at Urbana-Champaign (UIUC), in 1995 and 1998, respectively.

From 1998 to 2000, he was a Research and Development Engineer with the Ansoft Corporation, Pittsburgh, PA. Since 2000, he has been a faculty member with the Department of Electrical Engineering, University of Washington, Seattle, where he was an Assistant Professor from 2000 to 2005, and is currently a Tenured Associate Professor. He directs the Applied Computational Engineering (ACE) Laboratory, which has received research funding from the Defense Advanced Projects Agency (DARPA), National Science Foundation (NSF), Semiconductor Research Corporation (SRC), Intel Corporation, IBM, National Aeronautics and Space Administration (NASA), Air Force, Navy, Lawrence Livermore, the Small Business Innovation Research (SBIR) program, and the State of Washington. He is currently on partial leave from the University of Washington, while serving as founder and CEO of Physware Inc, Bellevue, WA, a venture-funded startup producing electronic design automation tools for microelectronic simulation and design. He has served as a consultant and reviewer for NASA, Department of Defense (DoD), NSF, Science Foundation Ireland, Cadence Design Systems, McGraw-Hill, Prentice-Hall, Kluwer, Cambridge University Press, and Calypso Medical. He has authored or coauthored approximately 150 papers in journals and refereed conference proceedings. His research interests include computational electromagnetics, integral equations, fast multilevel algorithms, parallel computation techniques, circuit and system applications of field solvers, signal and power integrity, electromagnetic interference (EMI)/electromagnetic compatibility (EMC), multiphysics and hierarchical simulation methods, RF identification (RFID) systems, statistical and design techniques for field solvers, and graph theory applications of field techniques.

Dr. Jandhyala is a full elected member of URSI Commission B. He was a recipient of a 2008 NASA Patent Inventor Award, a 2004 Outstanding Graduate Research Advisor Award from the Department of Electrical Engineering, University of Washington, a 2001 NSF CAREER Award, a Raj Mittra Oustanding Graduate Research Award presented by UIUC in 1998, and an IEEE Microwave Theory and Techniques Society (IEEE MTT-S) Graduate Fellowship in 1997.

Authorized licensed use limited to: University of Washington Libraries. Downloaded on July 13, 2009 at 15:12 from IEEE Xplore. Restrictions apply.